Al-doped maghemite examined as catalyst for the discoloration of methylene blue and for the decomposition of ammonium nitrate

A. F. Cabrera, C. E Rodríguez Torres and S. J. Stewart[#]

IFLP-CCT-La Plata-CONICET and Departamento de Física, Facultad de Ciencias Exactas, Universidad Nacional de La Plata, C. C. 67, 1900 La Plata, Argentina

[#]Corresponding author: stewart@fisica.unlp.edu.ar

Abstract

Nanostructured aluminium-doped magnetic iron (III) oxide ($Al_xFe_{2-x}O_3$ with x= 0.33, 0.67 and 1) have been prepared by autocombustion method. The as-prepared samples were characterized by XRD, thermogravimetric analysis, UV-vis and Mössbauer spectroscopies and magnetometry. The cubic spinel is the main crystalline phase for all compositions. The presence of Al in the spinel phase causes a progressive decrease in both the cell parameter (a) *a*nd the grain size (L). The room temperature Mössbauer spectrum of x= 0.33 is mainly composed of a Fe^{3+} broad sextet while, for higher Al content, the spectra consist of a Fe^{3+} broad doublet corresponding to superparamagnetic maghemite. The saturation magnetization decreases with the Al doping and reaches a rather low value for the ill-crystalline sample x = 1 (M_S ~ 2 emu/g). The optical direct band gap of the samples is red-shifted with respect to pure maghemite, with values close to 2 eV. The photocatalytic performance of $Al_xFe_{2-x}O_3$ tested in the decolorization of methylene blue dye showed a good efficiency for the oxide whose band gap energy best matches the energy of the incident light (x= 0.33). The catalytic effect of these samples on the thermal decomposition of ammonium nitrate is more noticeable for those Al concentrations that lead to the reaction being exothermic.

Keywords: maghemite, Al-doped Fe_2O_3, photocatalysis, propelents, methylene blue, ammonium nitrate

Introduction

Magnetic iron oxide (Fe_3O_4, γ-Fe_2O_3) nanomaterials have been widely studied for their basic interest and great potential for multiple applications such as energy conversion and storage, biomedicine, catalysis, solar fuels, water separation, and environmental remediation [1-6]. The search for possible applications of these materials continues intensely, being strongly encouraged by its unique properties such as biocompatibility, abundance of constituent elements, low cost, non-toxicity, environmentally friendly material, narrow band gap and good magnetic response to promote recovery and recycling processes. As nanosystems, the large surface-volume ratio makes them particularly suitable as catalysts for certain reactions taking advantage of their semiconductor properties and the surface modification that results from the local disorder or by the incorporation of impurities doping.

Amongst iron oxides, maghemite (γ-Fe_2O_3) is a cation-deficient spinel ferrite also expressed as $Fe_{8/3}\square_{1/3}O_4$, where $\square$ represents a cation vacancy. The Fe(III) ions distribute among both the tetrahedral A and octahedral B spinel interstitial sites resulting from the close-packed oxygens, while the vacancies are usually allocated at B sites but can also occupy A sites [1,7]. The distribution of iron vacancies varies with the preparation method and, depending on the vacancy ordering, γ-Fe_2O_3 crystallizes into different symmetries [8,9]. Like magnetite (Fe_3O_4), γ-Fe_2O_3 is ferrimagnetic with a high saturation magnetization at room temperature (74-80 emu/g), being both iron oxides, the most important magnetic minerals in soils and sediments [10]. However, natural pure maghemite is not available because it usually contains substitutional metal cations like Ti^{4+}, Mg^{2+} or Al^{+3} among others [10]. Since γ-Fe_2O_3 is a metastable phase, the methods used to synthesize this compound must be adequate to avoid the formation of the most thermodynamically stable Fe(III) oxide, i. e., weakly ferromagnetic hematite (α-Fe_2O_3). Thus, oxidation of magnetite or dehydration of ferric hydroxides are usual procedures to obtain nanosized γ-Fe_2O_3 [11], but methods like co-precipitation, solvothermal, hydrothermal, microemulsion and sol-gel combustion processes have also been employed [1,2,12]. In recent years, the low-temperature autocombustion process has attracted increasing attention in the manufacture of ceramic oxides nanopowders including

spinel ferrites due to its environmentally friendly, easy-to-implement, and low-cost synthesis pathway [13,14].

One way to improve the performance of γ-Fe_2O_3 nanoparticles as catalysts or photocatalysts can be achieved by doping the oxide with other metals to produce slight modifications in its semiconductor characteristics, such as a change of the transitions from the bandgap to the visible region and/or to delay the mechanism of recombination of electron-hole pairs thus encouraging the green chemistry [1,6,12]. Taking into account that the presence of tiny amounts of aluminium ions helps to stabilize the natural formation of maghemite, we employ the autocombustion method to synthesize nanostructured Al-doped maghemite ($Al_xFe_{2-x}O_3$ with x= 0.33, 0.67 and 1) for applications as a catalyst or photocatalyst. The samples were characterized using several techniques (x-ray diffraction, thermal analysis, Mössbauer spectroscopy, magnetometry, UV-vis spectroscopy). To explore possible technological applications these Al-doped iron oxides were tested as catalysts for the degradation of methylene blue (MB) as well as oxidant for the thermal decomposition of ammonium nitrate (AN).

2. Experimental

2. 1 *Sample preparation*

The synthesis of Al-doped maghemite powders was performed by autocombustion method [13]. Commercial powders of $Al(NO_3)_3$-$9H_2O$ and $Fe(NO_3)_3$-$9H_2O$ nitrates and citric acid $C_6O_7H_8$ (Biopack) were mixed in stoichiometric proportions to obtain $Al_xFe_{2-x}O_3$ samples with x= 0.33, 0.67 and 1. Mixtures of Al and Fe nitrates and acid citric were heated on a hot-plate under continuous stirring until gelification took place. Then, the gel was kept at approximately 80 ºC until the combustion occurred. Each sample was ground in an agate mortar until the mixture was homogeneous and then subjected to a heat treatment at 200 ºC for 2 hours in air.

2. 2 *Characterization techniques*

X-ray diffraction (XRD) measurements were carried out on a Philips Instrument PW 1710, operating with Cu Kα radiation (λ = 1.5406 Å) and employing a scan rate of 0.02 degrees per second in the scattering angular range (2θ) of 20–80 degrees. The lattice parameter values (a) and average crystallite sizes (*L*) were obtained using MAUD software [15].

The Mössbauer spectra of samples were measured in the transmission geometry at room temperature using a source with a nominal 50 mCi ^{57}Co source in Rh matrix with a linear velocity. The data were processed using the Recoil program [16]. Isomer shifts (IS) are referred to metallic α-Fe at room temperature.

DC-magnetic measurements at 300 K were performed using a vibrating sample magnetometer (Quantum Design).

Thermogravimetric (TGA) and differential scanning calorimetric (DSC) measurements were carried out in a Shimadzu-TGA50 and DSC-50, respectively, under nitrogen atmosphere (20 ml/min) in the 25 to 650 ºC temperature range with a heating rate of 10 ºC/min. The magnetic ordering temperature of samples x=0 and 0.33 were determined from the mass-loss difference during TGA running with and without an applied magnetic field of *H*= 8 mT. Attempts to determine the ordering temperature of samples x=0.67 and 1 were unsuccessful due to the low magnetic response of these samples under 8 mT.

2. 3 *Experimental setups to test the catalytic performance of γ-$Al_xFe_{2-x}O_3$ for the degradation of methylene blue and for the decomposition of ammonium nitrate.*

The photoinduced degradation of methylene blue (MB) dye in the presence of $Al_xFe_{2-x}O_3$ catalysts was evaluated using UV-vis absorption registered through a spectrophotometer model Shimadzu UV 2600. Aqueous suspensions containing 12 ppm of MB (0.8 mg/ml) were continuously mixed using a sonicator and illuminated with visible light generated by a 9 W (3000 K) light-emitting diode (LED) lamp placed at 20 cm above the liquid. Every 10 minutes a small aliquot of the liquid was separated and placed in a spectrophotometer cell, after decanting the magnetic particles using a magnet. The absorption curve was registered in a wavelength range between 300 and 850 nm.

To test $Al_xFe_{2-x}O_3$ as catalysts for the thermal decomposition reaction of ammonium nitrate (AN), mixtures AN + $Al_xFe_{2-x}O_3$ were prepared using a 95:5 AN:$Al_xFe_{2-x}O_3$ mass ratio and mixed in an agate mortar. Afterwards, an amount of 200 mg of these mixtures were placed in a stainless-steel cylinder of about 0.6 cm^3. A Sieverts type apparatus was used to carry out the thermal treatments in this closed reactor, whose setup allows measurement of instantaneous pressure and temperature as function of time (see Ref. [17] for details).
The AN thermal decomposition was also investigated using the DSC technique, where AN + $Al_xFe_{2-x}O_3$ mixtures were placed in a platinum crucible with an open pan under the heating conditions described in the subsection 2.2.

3. Results and Discussion

3. 1 Structural, hyperfine, magnetic and optical spectroscopic characterization of $Al_xFe_{2-x}O_3$ catalysts

Figure 1 shows the XRD diffractograms of Al-doped maghemite samples; the pattern of 30 nm γ-Fe_2O_3 nanoparticles (NPs) studied in Ref. [18] is also included for comparison. We observe that all the patterns show the Bragg reflections corresponding to cubic spinel (Space Group *Fd3m*) [9]. Extra peaks belonging to hematite as a secondary phase are also detected (see Fig. 1). We observe that both *a* and *L* decrease with increasing the aluminium content (Figs. 2(a) and 2 (b)). Moreover, the detriment of *a* by about 2.5 % when x=1 is almost in agreement with the value predicted by Vegard's law for ideal solutions (see Fig. 2 (a)). These results are similar to those previously reported for Al-doped maghemite [7,19,20] (Fig. 2(a)), and they are expected considering the inclusion of Al^{3+} ions at cationic spinel sites with lower ionic radius than Fe^{3+}. Similarly, to previous findings, our results indicate that the inclusion of Al prevents the grain size growth of the oxide (Ref. [7] and references therein). Indeed, we observe that increasing x=0.33 up to x=1 reduces the spinel crystallite size by a quarter. Moreover, the rather broad and poorly defined Bragg peaks for sample x=1 indicate its ill-defined long-range structure. It is worth mentioning that attempts to synthesize a sample without Al content (x=0) throughout the autocombustion method as described here have been unsuccessful.

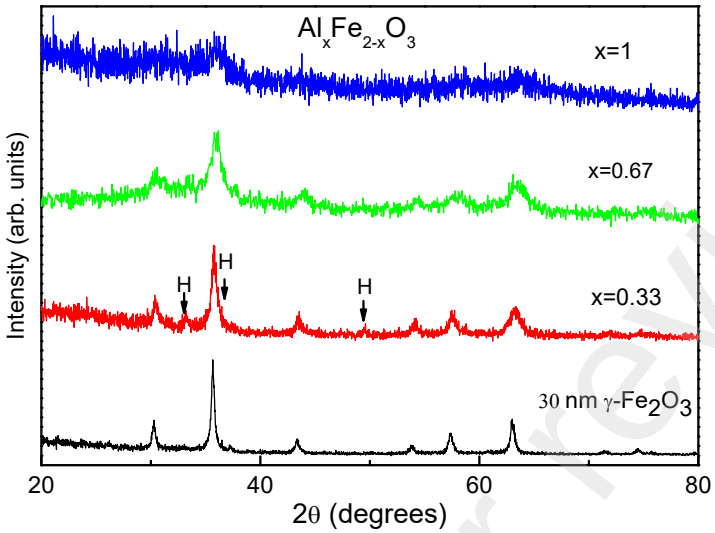

Figure 1: XRD diffractograms of $Al_xFe_{2-x}O_3$ samples. The pattern of 30 nm γ-Fe_2O_3 nanoparticles (Ref. [18] is also included. The arrows indicate the visible Bragg peaks of hematite α-Fe_2O_3 (H).

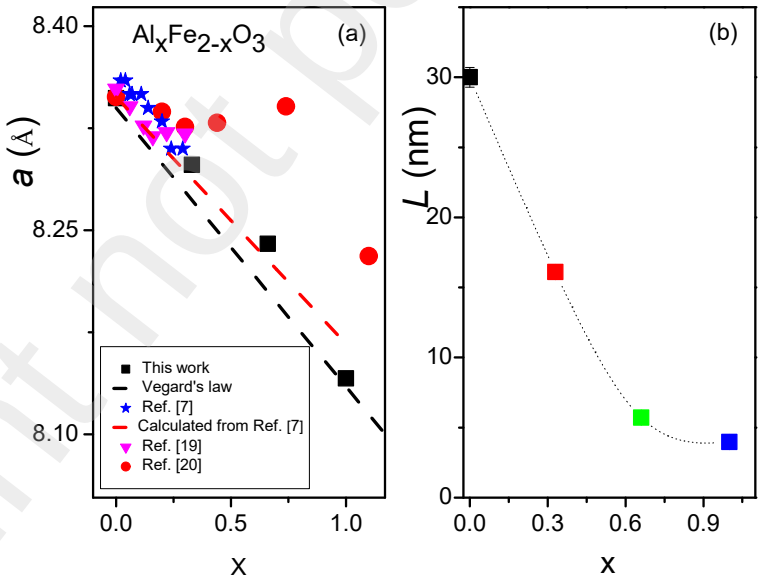

Figure 2: (a) Cell parameter (*a*) for the different Al-content (*x*). The figure also includes data from Refs. [7,19,20]. The linear behaviour predicted by Vegard's law is also shown (black dashed line). (b) Average crystallite size (*L*) as a function of the aluminium content (*x*). The dash line was added for the eye guide. The *x*= 0 value corresponds to the 30 nm γ-Fe_2O_3 sample (Ref. [18]).

Previous studies on bulk γ-Fe_2O_3 have reported that its room temperature zero-field Mössbauer spectrum consists of a broad asymmetric sextet (see, for instance, [21]), which accounts for the superposition of hyperfine magnetic fields belonging to Fe^{3+} at both A and B sites [21]. The similar hyperfine parameters of Fe^{3+} at A and B sites added to the random location of cation vacancies resulting in different iron environments makes it difficult to determine the A and B contribution separately unless in-field Mössbauer experiments were performed [22]. On the other hand, surface and size effects in nanosized γ-Fe_2O_3 or the partial substitution of iron by another cation can also cause line broadening and line-shape asymmetry [21]. Thus, to account for the different iron local environments the spectra need to be fitted assuming several magnetic components with distribution of hyperfine fields. Figure 3 shows the Mössbauer spectra of Al-doped maghemite obtained by autocombustion. Spectrum belonging to nanosized γ-Fe_2O_3 is also included, the latter showing a broad sextet that was fitted to six distributed magnetic components (Table I). Spectrum of $Al_{0.33}Fe_{1.67}O_3$ (x=0.33) is composed of a magnetic signal, which is fitted to three distributed magnetic sextets plus a broad doublet. The two distributed sextets with high hyperfine field (B_{hf}) values can be assigned to Fe mainly occupying spinel sites in a blocked state, while the sextet with B_{hf} of about 200 Oe with no direct physical sense was included to account for iron atoms at particles whose relaxation times are comparable to the Mössbauer time scale (about 10^{-8} s). For high Al content (x= 0.67 and 1) no magnetic resolved lines are observed and each spectrum mainly consists of a broad Fe^{3+} doublet fitted to a distribution of quadrupolar sites. The latter corresponds to Fe^{3+} belonging to maghemite and, to a lesser extent, to the hematite secondary phase both in a superparamagnetic relaxation state within the Mössbauer time scale. Additionally, a minor component with a large IS needs to be included to fit the spectra of x = 0.67 and 1.

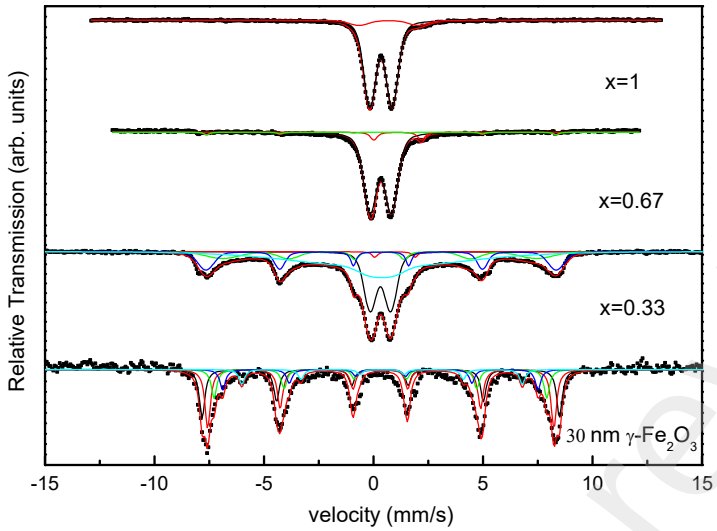

Figure 3: Mossbauer spectra at 298 K. The solid lines are the result of the fitting procedure.

Table I: Mössbauer hyperfine parameters resulting from the fitting procedure. δ in the isomer shift, ΔQ is the quadrupole shift or quadrupolar moment, B_{hf} is the hyperfine field, σ is the distribution width, A is the relative area.

Sample	δ (mm/s)	ΔQ(mm/s)	B_{hf} (Oe)	σ mm/s)	A (%)
γ-Fe_2O_3 NPs	0.31_1	0.02_1	506_1	0.3	28.1
x=0	0.32_1	0.009_8	490_1	0.3	34.2
	0.31_2	0	471_2	0.3	16.8
	0.31_2	-0.01_2	446_2	0.3	12.1
	0.39_3	0	397_2	0.6	8.7
$Al_xFe_{2-x}O_3$	0.315_5	0.94_1		0.46_1	24
	0.28_1		445_{13}	44_{10}	13
x=0.33	$0,34_1$		496_1	19_2	19
	0.36_3		203_{17}	204_{20}	42
x=0.67	0.329_2	0.974_4		0.464_6	91.16
	1.09_2	2.16_4		0.15_5	5.7
x=1	0.340_1	1.024_3		0.432_3	91.65
	0.69_3	2.72_7		0.77_8	8.35

The values of saturation magnetization (M_S) at room temperature reported for bulk γ-Fe_2O_3 is about 74-80 emu/g and, as a magnetically soft material, it presents a small coercivity field (H_C)[23]. Due to finite-size and surface effects a reduction of M_S is expected for nanosized maghemite [23]. This is observed for 30 nm-γ-Fe_2O_3 (Fig. 4), whose M_S (determined at the maximum applied field) is nearly 60 emu/g while H_C is about 9 Oe. Figure 4 also shows the loops of Al-substituted samples. We observe a progressive decrease of M_S with the Al content, reaching a rather low value for the ill-crystalline x = 1 sample ($M_S \sim 2$ emu/g). A similar behavior was found by Batista *et al*. [7] for high levels of Al-isomorphous substitution. The inclusion of non-magnetic Al^{+3} ions in the maghemite lattice generates a weakening of superexchange interactions, which produces a reduction of the magnetic ordering temperature of maghemite (Fig. 5) and reduces M_S. In the present case, the decrease of M_S is also affected by the L detriment caused by the addition of aluminium and, additionally, by the presence of a small amount of the hematite phase detected by XRD. The negligible hysteresis in the M *vs.* H loops of x = 0.67 and 1 samples (see inset Fig. 4) indicates that the particles are in a superparamagnetic state (within an experimental time scale of about 100 s).

Figure 5 shows the difference between the TG thermal measurements with and without the presence of a magnetic field (ΔTG) for pure maghemite nanoparticles and Al-doped maghemite (x=0.33). This can be used to determine the magnetic ordering temperature (T_C) of the material considering that as it is heated in the presence of H near T_C there will be an apparent weight loss when the magnet no longer attracts the sample. In both cases, T_C is within the range of values reported in the literature for maghemite, viz. 743 K to 985 K [21,24]. However, T_C decreases with the addition of Al (T_C is around 890 K for the non-substituted sample, while is around 860 K for x=0.33). To our knowledge there has been no other direct determination of the ordering temperature for Al-doped maghemite, this being restricted to indirect measurements using Mossbauer spectroscopy [19].

The optical reflectance spectra are shown in Fig. 6 (a). It is noteworthy that higher reflectance values of the Al-doped samples are shifted towards the high wavelength optical region when they are compared with the results of pure maghemite nanoparticles. The energy band gaps (E_G) of these nanomaterials (see Fig. 6 (c)) were obtained from application of the Tauc Plot

method and considering direct transitions [25,26]. We observe that the band gap of about 2.6 eV for 30 nm-γ-Fe_2O_3 nanoparticles is blue-shifted with respect to the values reported for bulk maghemite (2.0 eV), and this can be due to its nanometric grain sizes [27,28]. On the contrary, E_G values near 2 eV are registered for the also nanosized Al-doped maghemites (x= 0.33 and 0.67), while the x=1 sample shows an appreciable red-shift in the band gap transition. Thus, even though the L sizes of Al-doped maghemites are lower than pure nanosized maghemite (Fig. 2 (a)), the inclusion of aluminium modifies the electronic configuration and counteracts the size effect on the band gap transition.

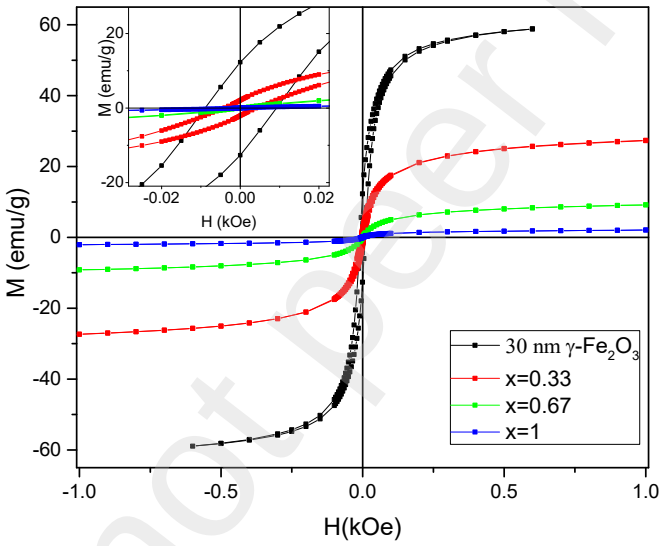

Figure 4: Magnetization versus applied magnetic field curves taken at 298 K. Inset: Enlargement of the loops at low magnetic fields.

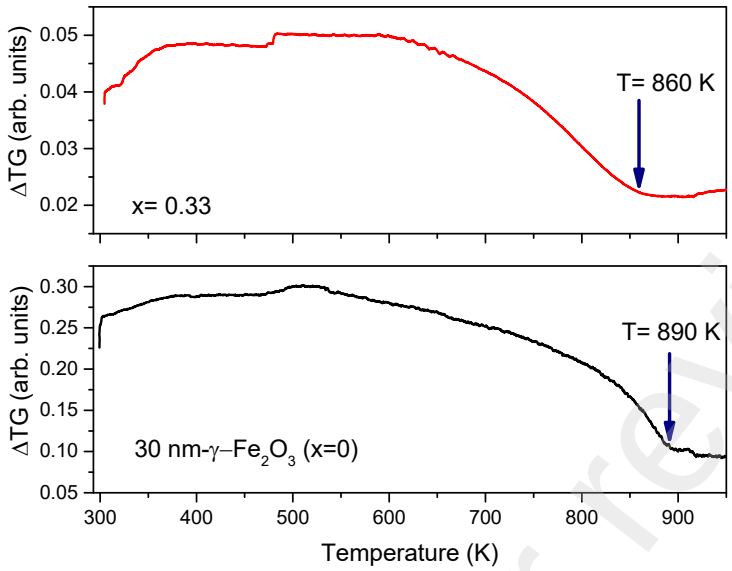

Figure 5: Difference between TGA curves recorded with and without an applied magnetic field of 8 mT.

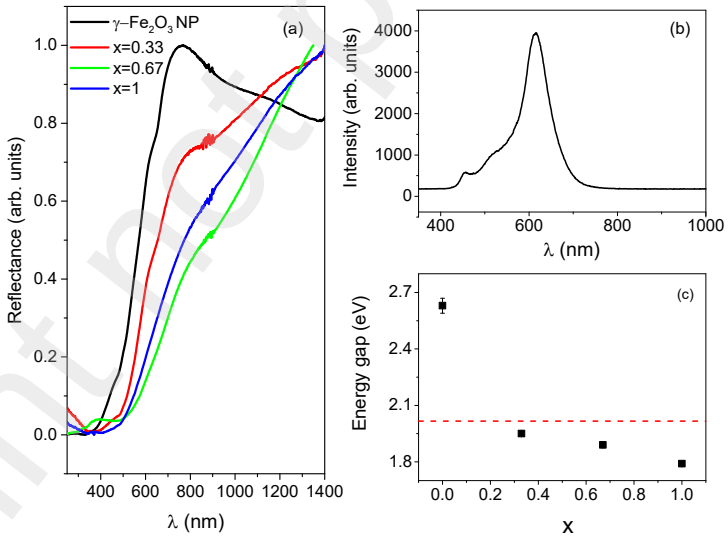

Figure 6: (a) Reflectance against wavelength in the range 200–1400 nm for a set of Al-doped Fe_2O_3 samples, (b) Light intensity of the LED lamp as a function of the wavelength, (c) Direct optical band gap energy (E_G) values. The red dotted line indicates the energy of maximum intensity of the incident light.

3. 2 Photocatalytic performance of $Al_xFe_{2-x}O_3$ on the MB degradation

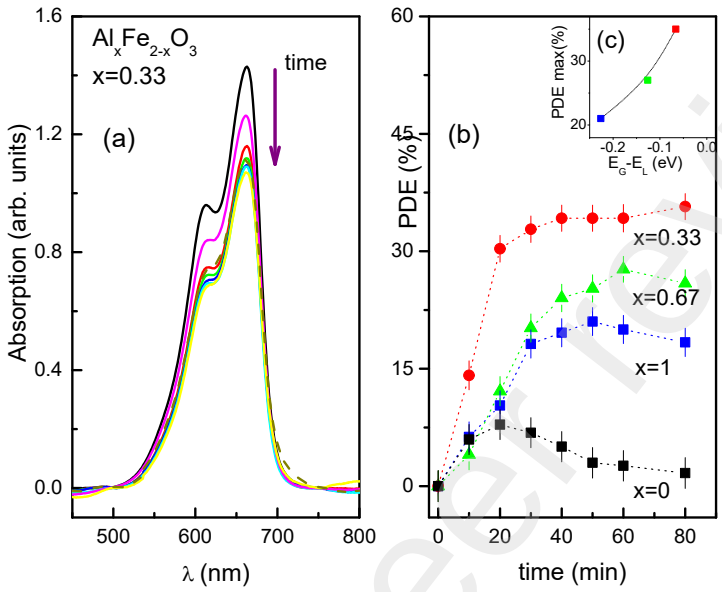

Figure 7: (a) Photocatalytic degradation of methylene blue (MB) plus $Al_xFe_{2-x}O_3$ (x=0.33) catalyst aqueous solution under visible light irradiation. (b) Photodegradation efficiency percentage (PDE%) as defined in the text (Inset (c) Maximum PDE% as a function of the difference between the energy band gap E_G of Al-doped samples and the energy of the incident light E_L).

The absorbance spectra (Fig. 7 (a)) show two broad peaks at about 609 and 665 nm corresponding to the characteristic absorption bands of MB [25,29]. A decrease of the absorption intensity with the exposure time is observed for all Al-doped samples (Fig. 7(b)). The MB degradation is also confirmed by visualising the progressive discoloration of the solution. Figure 7 (b) shows the photocatalytic degradation efficiency percentage (PDE%) estimated by using the expression PDE% = 100 x (1 - I_{MBtS}/I_{MB}), where I_{MBtS} and I_{MB} are the highest peak intensities of the spectra of the supernatant of MB + catalyst mixtures and pure MB, respectively, after a time interval *t*. These results show that the catalytic performance improves in the way x=1→0.67→0.33.

As previously reported [25], the exposed surface area of the catalyst and the presence of carbonaceous residuals in samples prepared by autocombustion influence the photoactivated degradation process of MB. On one hand, visible light irradiation promotes the generation of electron-hole pairs in these oxides that favours its photocatalytic activity. On the other hand, the carbon remnants inhibit the recombination process. This can explain the higher PDE% reached for Al-doped samples in comparison with pure maghemite nanoparticles, as shown in Fig. 7 (b). However, there is a lack of correlation between the *L* sizes and PDE% of $Al_xFe_{2-x}O_3$, considering that the x= 0.33 sample is the one presenting the best performance. It is worth noting that the estimated direct band-gap value for this sample is closest to the energy value of the incident light (2.01 eV) (Fig. 6 (b)), thus the absorption of light facilitates the promotion of electrons to the conduction band.

3. 2 Influence of the additives $Al_xFe_{2-x}O_3$ on the thermal decomposition of ammonium nitrate

Nanostructured transition metal oxides have been proved to be effective additives to the thermal decomposition of ammonium nitrate [30]. In a previous work [17], we demonstrated that the incorporation of MFe_2O_4 (M = Mg, Co, Cu, and Zn) spinel ferrites prepared by autocombustion decreases the onset temperature of the process that manifests itself through an exothermic reaction and, in addition, increases the amount of heat released during the reaction. Further, the catalytic performance of these ferrites can be correlated with the electronegativity of M^{2+} cations, which act as Lewis acid sites that interact with the gas molecules removing ammonia.

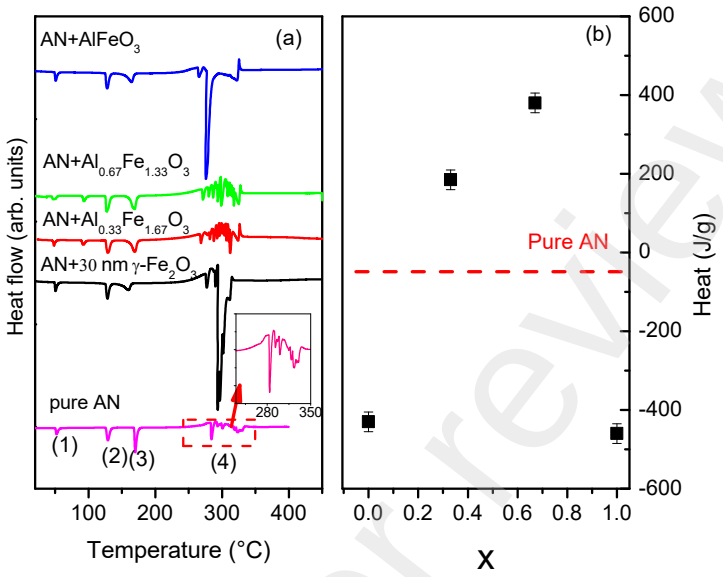

Figure 8: (a) DSC curves for pure AN and AN + $Al_xFe_{2-x}O_3$ mixtures placed in a sealed aluminium pan, (b) Heat released during the AN decomposition as a function of the aluminium content.

To test the effect of $Al_xFe_{2-x}O_3$ as a catalyst on the thermal decomposition of AN we have employed usual techniques for thermal analysis as well as through thermal treatments in a closed reactor. The DSC curve of pure AN under sealed condition shows endothermic peaks related to structural phase transformations (peaks (1) and (2) in Fig. 8 (a)), and peak (3) that corresponds to the melting of AN. The labelled peak (4) corresponds to the thermal decomposition of AN [31]. Further, near the peak (4) region (see inset Fig. 8 (a)) we observe oscillations due to the superposition of endothermic and exothermic peaks, which account for the AN decomposition (into HNO_3 and NH_3) and an oxidation reaction, respectively [17]. With the addition of the catalyst, while the first two DSC peaks remain unaltered, peak (3) broadens and shifts to lower temperatures. We observe that the incorporation of nanosized maghemite makes the decomposition reaction more endothermic (Figs. 8 (a) and (b)). Interestingly, this same behavior is observed for the sample with the highest Al content (x=1), while for x=0.33 and 0.67 an exothermic reaction predominates (see Fig. 8 (b)).

Figure 9 (a) shows the pressure chamber (P) recorded during the thermal decomposition of AN and AN + catalyst carried out in the reactor. The decomposition is reflected by the

increase of *P*, which for pure AN starts around 200 ºC and extends for about an interval of about 170 ºC. While the addition of 30 nm-γ-Fe_2O_3 or $AlFeO_3$ (x=1) shifts the decomposition towards higher temperatures, this effect is not observed for x=0.33 and 0.67 samples. However, the catalytic influence of these samples is manifested in the rate of change of pressure (*dP/dt*), shown in Fig. 9 (b), where the maximum rate is registered adding x=0.67 sample.

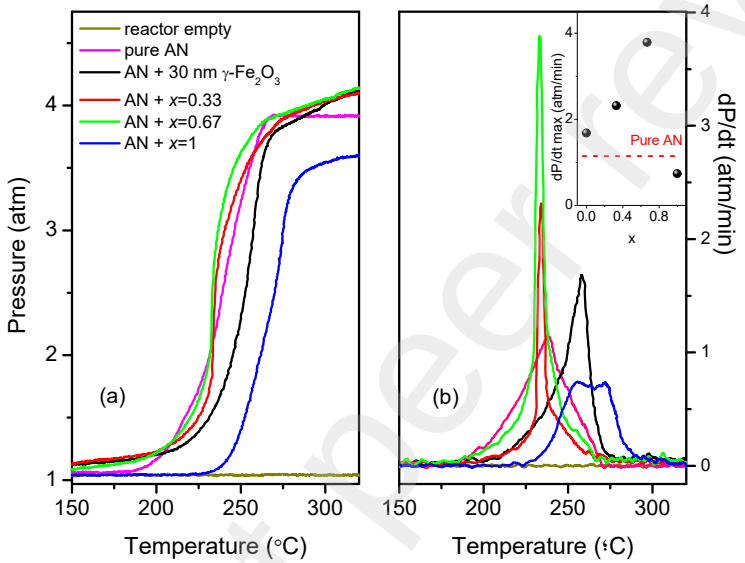

Figure 9: (a) Pressure (*P*) as a function of the temperature reactor chamber for pure AN and AN + catalysts mixtures. (b) Rate of change of pressure (*dP/dt*) *versus* the temperature reactor chamber for pure AN and AN + catalysts mixtures (Inset: Maximum values of the pressure velocity registered for each sample).

Hence, our results indicate that the addition of 30 nm-γ-Fe_2O_3 or $AlFeO_3$ delays the onset temperature of the decomposition reaction, being the latter predominantly endothermic. On the contrary, the incorporation of $Al_xFe_{2-x}O_3$ (x= 0.33, 0.67) makes the reaction more exothermic and, at the same time, leads to a higher reaction rate without appreciable changes of the onset temperature (see Fig. 10). Furthemore, the catalytic effect of these Al-doped maghemites follows the same trend previously observed for other spinel compounds, i. e., it can be correlated with the generalized electronegativity $\chi i = (1 + 2Z)\chi_0$ (χ_0 is the Pauling's electronegativity of the metal element and Z is the valence of metal ions (see Ref. [17] and

references therein)), being $\chi i = 11.27$ for Al^{3+}. According to this interpretation, the metal cations participate as acidic Lewis sites to remove ammonia in the AN decomposition process throughout an exothermic oxidation reaction with nitric acid and its reaction products. Finally, the results indicate that the effect of these Al-doped maghemites in this decomposition process is not directly related to the size of the particles but to the concentration of aluminium for which the reaction becomes exothermic.

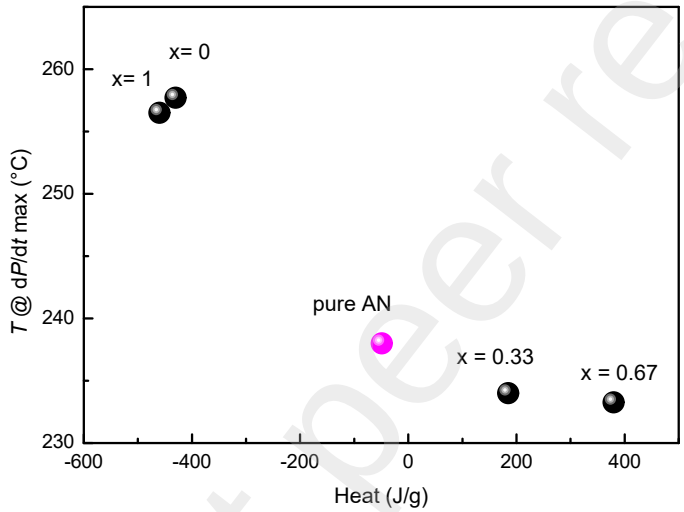

Figure 10: Temperature at which the maximum change of pressure (*dP*/*dt* max) is registered in the reactor versus the heat released during the decomposition from DSC experiments.

4. Conclusions

Nanoparticles of aluminium-doped maghemites were successfully prepared by autocombustion method. The XRD patterns exhibited diffraction peaks corresponding to a cubic spinel structure with average crystallite size and lattice parameter that decrease with the aluminium content. The Mossbauer studies revealed that the oxidation state of the iron ions was 3+, while the magnetic results showed the ferrimagnetic character of the samples, leading to the conclusion that iron atoms form the maghemite phase, in agreement with XRD results. The energy band gap of the samples is red-shifted with the Al content, going from 2.6 eV (x=0) to 1.8 eV (x=1). The values of the energy band make $Al_xFe_{2-x}O_3$ suitable

magnetic materials for the recovery of contaminated water. The addition of Al increases the surface-volume ratio, which, added to the presence of carbonaceous residues produced by the autocombustion method, influences the effectiveness of $Al_xFe_{2-x}O_3$ as a photocatalyst in the degradation of the methylene blue dye. The best photocatalytic degradation efficiency was observed for the sample x=0.33, whose direct band-gap energy value matches the energy of the incident light. Although by controlling the content of Al we can tune the band gap to the incident energy to, doping magnetic iron (III) oxide with Al^{3+} does not seem to be the most suitable for the photodegradation of methylene blue because low levels of degradation are reached. Finally, for the application of Al-doped maghemites as catalysts for the decomposition reaction of ammonium nitrate, samples x= 0.33 and 0.67 are the most suitable since they produce exothermic reactions at lower temperatures than pure maghemite.

Acknowledgements

This work was supported by CONICET and UNLP, Argentina.

Compliance with Ethical Standards:

Conflict of Interest: The authors declare that they have no conflict of interest.

References

[1] H. J. Shokrollahi, H.J., A review of the magnetic properties, synthesis methods and applications of maghemite. J. Magn. Magn. Mat. 426 (2017) 74-81. https://doi.org/10.1016/j.jmmm.2016.11.033

[2] S. Laurent, D. Forge, M. Port, A. Roch, C. Robic, L. Vander Elst, R. N. Muller, Magnetic iron oxide nanoparticles: synthesis, stabilization, vectorization, physicochemical characterizations, and biological applications. Chemical Reviews, 108 (2008) 2064-2110. https://doi.org/10.1021/cr068445e

[3]T. Tuutijärvi, J. Lu, M. Sillanpää, G. Chen, As (V) adsorption on maghemite nanoparticles. J. Hazardous Materials, 166 (2009) 1415-1420. https://doi.org/10.1016/j.jhazmat.2008.12.069

[4] J. Hu, G. Chen, I. M. Lo,. Removal and recovery of Cr (VI) from wastewater by maghemite nanoparticles, Water Research, *39* (2005) 4528-4536. https://doi.org/10.1016/j.watres.2005.05.051

[5] E. M. Múzquiz-Ramos, V. Guerrero-Chávez, B. I. Macías-Martínez, C. M. López-Badillo, L. A. García-Cerda, Synthesis and characterization of maghemite nanoparticles for hyperthermia applications, Ceramics International 41 (2015) 397-402. https://doi.org/10.1016/j.ceramint.2014.08.083

[6] A. Rehman, A. Daud, M. F. Warsi, I. Shakir, P. O. Agboola, M. I. Sarwar, S. Zulfiqar, Nanostructured maghemite and magnetite and their nanocomposites with graphene oxide for photocatalytic degradation of methylene blue, Materials Chemistry and Physics, *256* (2020) 123752. https://doi.org/10.1016/j.matchemphys.2020.123752

[7] M. A. Batista, A. C. Costa, J. M. Bigham, A. Paesano Junior, G. Berndt G, T. T. Inoue, A. G. Nonaka, Structural and magnetic characterization of maghemites prepared from Al-substituted magnetites. Revista Brasileira de Ciência do Solo 37 (2013) 1569-1575. https://doi.org/10.1590/S0100-06832013000600013

[8] T. Belin, N. Guigue-Millot, T. Caillot, D. Aymes, J. C. Niepce, Influence of grain size, oxygen stoichiometry, and synthesis conditions on the γ-Fe_2O_3 vacancies ordering and lattice parameters. J. Solid State Chem., 163 (2002) 459-465. https://doi.org/10.1006/jssc.2001.9426

[9] J. E. Jorgensen, L. Mosegaard, J. C. Hanson, T. R. Jensen, L. E. Thomsen, Formation of γ-Fe_2O_3 nanoparticles and vacancy ordering: an in situ x-ray powder diffraction study, J. Solid State Chem. 180 (2007) 180-185, https://doi.org/10.1016/j.jssc.2006.09.033

[10] C. E. Mullins, Magnetic susceptibility of the soil and its significance in soil science–a review, J. Soil Sci. 28 (1977) 223-246. https://doi.org/10.1111/j.1365-2389.1977.tb02232.x

[11] M. Aliahmad, N. Nasiri Moghaddam, Synthesis of maghemite (γ-Fe_2O_3) nanoparticles by thermal-decomposition of magnetite (Fe_3O_4) nanoparticles, Materials Science-Poland 31 (2013) 264-268. https://doi.org/10.2478/s13536-012-0100-6

[12] Y. L. Pang, S. Lim, H. C. Ong, and W. T. Chong, Research progress on iron oxide-based magnetic materials: synthesis techniques and photocatalytic applications, Ceramics International, 42 *(*2016) 9-34. https://doi.org/10.1016/j.ceramint.2015.08.144

[13] C. Hwang, T. Wu, J. Wan, J. Tsai, Development of a novel combustion synthesis method for synthesizing ceramic oxide powders, Mater. Sci. Eng. B 111 (2004) 49–56, https://doi.org/10.1016/j.mseb.2004.03.023.

[14] A. S. Džunuzović, N. I. Ilić, M. V. Petrović, J. D. Bobić, B. Stojadinović, Z. Dohčević-Mitrović and B. D. Stojanović, Structure and properties of Ni–Zn ferrite obtained by auto-combustion method. J. Magn. Magn. Mat. 374 (2015) 245-251. https://doi.org/10.1016/j.jmmm.2014.08.047

[15] L. Lutterotti and P. Scardi, Simultaneous structure and size–strain refinement by the Rietveld method. J. Appl. Crystallography 23 (1990) 246-252. https://doi.org/10.1107/S0021889890002382

[16] D. G. Rancourt, J. Y. Ping, Voigt-based methods for arbitrary-shape static hyperfine parameter distributions in Mössbauer spectroscopy, Nuclear Instruments and Methods in Physics Research Section B: Beam Interactions with Materials and Atoms, 58(1) (1991), 85-97. https://doi.org/10.1016/0168-583X(91)95681-3

[17] A. F. Cabrera, C. E Rodríguez Torres, L. C. Juncal, M. Meyer, and S. J. Stewart. Effect of nanostructured ferrites MFe_2O_4 (M= Cu, Co, Mg, Zn) on the thermal decomposition of ammonium nitrate. Applications in Energy and Combustion Science 6 (2021) 100026. https://doi.org/10.1016/j.jaecs.2021.100026

[18] C. E. Rodríguez Torres, G. A. Pasquevich, P. M. Zélis, F. Golmar, S. P. Heluani, S. K. Nayak, W. A. Adeagbo, W. Hergert, M. Hoffmann, A. Ernst and P. Esquinazi, Oxygen-vacancy-induced local ferromagnetism as a driving mechanism in enhancing the magnetic response of ferrites, Phys. Rev. B, 89 (2014) 104411. https://doi.org/10.1103/PhysRevB.89.104411

[19] G. M. Da Costa , E. De Grave , L.H. Bowen , P.M.A. de Bakker, R.E. Vandenberghe, Temperature Dependence of the Hyperfine Parameters of Maghemite and Al-Substituted Maghemites, Phys Chem Minerals 22 (1995) 178-185. https://doi.org/10.1007/BF00202298

[20] G. M. Da Costa, C. Laurent, E. De Grave, R. Vandenberghe, A comprehensive study of highly-substituted aluminum magnemites. In Mineral spectroscopy: a tribute to RG Burns 5 (1996) 93-104. The Geological Society. http://hdl.handle.net/1854/LU-269195

[21] G. M. Da Costa, E. De Grave and R. E. Vandenberghe, Mössbauer studies of magnetite and Al-substituted maghemites. Hyp. Int. 117 (1998) 207-243. https://doi.org/10.1023/A:1012691209853

[22] T. J. Daou, J.M. Greneche, S. J. Lee, S. Lee, C. Lefevre, S. Bégin-Colin and G. Pourroy, Spin canting of maghemite studied by NMR and In-Field Mossbauer spectrometry. J. Phys. Chem. C 114 (2010) 8794-8799. https://doi.org/10.1021/jp100726c

[23] M. Coduri, P. Masala, L. Del Bianco, F. Spizzo, D. Ceresoli, C. Castellano, S. Cappelli, C. Oliva, S. Checchia, M. Allieta and D. V. Szabo, Local structure and magnetism of Fe_2O_3 maghemite nanocrystals: The role of crystal dimension, Nanomaterials 10 (2020) 867. doi:10.3390/nano10050867

[24] X. Liu, J. Shaw, J. Jiang, J. Bloemendal, P. Hesse, T. Rolph, X. Mao, Analysis on variety and characteristics of maghemite. Sci. China Earth Sci. 53 (2010) 1153–1162. https://doi.org/10.1007/s11430-010-0030-2

[25] A. F. Cabrera, C. E. Rodríguez Torres, S. G. Marchetti, S. J. Stewart, Degradation of methylene blue dye under dark and visible light conditions in presence of hybrid composites of nanostructured $MgFe_2O_4$ ferrites and oxygenated organic compounds, J. Environ. Chem. Eng. 8 (2020) 104274, https://doi.org/10.1016/j.jece.2020.104274

[26] M. Nowak, B. Kauch, P. Szperlich, Determination of energy band gap of nanocrystalline SbSI using diffuse reflectance spectroscopy, Rev. Sci. Instrum. 80 (2009) 046107. https://doi.org/10.1063/1.3103603

[27] L. P. Zhu, L. L. Wang, N. C. Bing, C. Huang, L. J. Wang, G. H. Liao, Porous fluorine-doped γ-Fe_2O_3 hollow spheres: synthesis, growth mechanism, and their application in photocatalysis. ACS Appl. Mat. Inter. 5 (2013) 12478-12487. https://doi.org/10.1021/am403720r

[28] I. M. Mirza, K. Ali, A. K. Sarfraz, A. Ali A. ul Haq, A study of dielectric, optical and magnetic characteristics of maghemite nanocrystallites. Mat. Chem. Phys. 164 (2015) 183-187. https://doi.org/10.1016/j.matchemphys.2015.08.041

[29] D. Heger, J. Jirkovsky, P. Klan, Aggregation of methylene blue in frozen aqueous solutions studied by absorption spectroscopy. J. Phys. Chem. A 109 (2005) 6702-6709. https://doi.org/10.1021/jp050439j

[30] J. A. Vara, P. N. Dave, Metal oxide nanoparticles as catalyst for thermal behavior of AN based composite solid propellant, Chem. Phys. Let. 730 (2019*)* 600-607. https://doi.org/10.1016/j.cplett.2019.06.048

[31] S. Chaturvedi, P. N. Dave, Review on thermal decomposition of ammonium nitrate, J Energ. Mater. 31 (2013) 1-26, https://doi.org/10.1080/07370652.2011.573523